Title	Efficiency enhancement in bulk-heterojunction solar cells integrated with large area Ag nano-triangle arrays
Author(s)	Wu, Bo; Oo, Than Zaw; Li, Xianglin; Liu, Xinfeng; Wu, Xiangyang; Yeow, Edwin Kok Lee; Fan, Hong Jin; Mathews, Nripan; Sum, Tze Chien
Citation	Wu, B., Oo, T. Z., Li, X., Liu, X., Wu, X., Yeow, E. K. L., et al. (2012). Efficiency enhancement in bulk-heterojunction solar cells integrated with large area Ag nano-triangle arrays. The Journal of Physical Chemistry C, 116(28), 14820-14825.
Date	2012
URL	http://hdl.handle.net/10220/8283
Rights	© 2012 American Chemical Society. This is the author created version of a work that has been peer reviewed and accepted for publication by The Journal of Physical Chemistry C, American Chemical Society. It incorporates referee's comments but changes resulting from the publishing process, such as copyediting, structural formatting, may not be reflected in this document. The published version is available at: DOI [http://dx.doi.org/10.1021/jp303672f].

Efficiency Enhancement in Bulk-Heterojunction Solar Cells Integrated with Large Area Ag Nano-Triangle Arrays

Bo Wu[1], Than Zaw Oo[2], Xianglin Li[1], Xinfeng Liu[1], Xiangyang Wu[2], Edwin Kok Lee Yeow[2], Hongjin Fan[1], Nripan Mathews[3,4] and Tze Chien Sum[1*]

[1]*Division of Physics and Applied Physics*, *School of Physical and Mathematical Sciences*, *Nanyang Technological University*, *Singapore 637371*, *Singapore*

[2]*Division of Chemistry and Biological Chemistry*, *School of Physical and Mathematical Sciences*, *Nanyang Technological University*, *Singapore 637371*, *Singapore*

[3]*Division of Materials Technology, School of Materials Science and Engineering, Nanyang Technological University, Singapore 639798, Singapore*

[4]*Energy Research Institute @ NTU (ERI@N), Singapore 637553*

ABSTRACT

Efficiency enhancement in plasmonic bulk heterojunction (PCDTBT:PCBM) organic solar cells (OSCs) is demonstrated with the integration of large area periodic Ag nano-triangle (NT) arrays (that were fabricated using the cost-effective, high throughput nanosphere lithography technique) in the OSC device. The improvements to the power conversion efficiency (from 4.24% to 4.52%) and to the short circuit current density (by ~12%) are attributed to an increase in exciton generation induced by the strong local E-field and the scattering generated by the localized surface plasmon resonance of the hexagonal NT arrays. These findings are validated by a range of steady state and transient optical spectroscopy and correlated with device performance data. Importantly, our work demonstrates the feasibility of integrating a simple cost-effective, tailorable and scalable nanofabrication technique with existing OSC fabrication processes.

KEYWORDS

Nanosphere lithography, Ag triangle array, surface plasmon, organic photovoltaics, charge dynamics

---

* Corresponding author: tzechien@ntu.edu.sg

1. Introduction

Organic photovoltaics (OPV) possess great potential as a renewable energy source due to their relatively low-cost and ease of fabrication.[1] One highly successful OPV design concept is based on the bulk heterojunction (BHJ) type of devices where power conversion efficiencies (PCE or η) exceeding ~7–8% have been reported.[2] Commercialization of OPV is expected once the efficiencies for single junction devices exceed 10%. However, intrinsic to organic systems, the low carrier mobilities limiting the active layer thickness impose severe constraints to the efficiency of OPV devices. Enhancing the absorbance with a thicker active layer typically leads to a rapid decrease of the internal quantum efficiency due to low carrier mobility and short exciton diffusion lengths of organic materials[3]; while thin active layers are inefficient due to poor absorbance. One promising approach out of this predicament would be to utilize plasmonic nanostructures (subwavelength plasmonic nanostructures[4-7] or periodic arrays or gratings[8-10] in OPV devices) to confine light within the active layer to promote absorption; thereby increasing the optical thickness of OPV materials for light harvesting. Plasmonic origins to the PCE improvement can be attributed to the increased light absorption in the active layer brought about either by strong scattering and/or waveguiding by the metal nanostructures that enhances the electromagnetic (EM) field in the active layer or by overlap of the strong plasmonic modal fields with the active layer. Of late, this approach has garnered substantial interest within the OPV community.

Despite its great potential, successful experimental demonstration of plasmonic enhancement in OPV remain far and few; and mired with controversy. Anomalous increase and decrease in PCE have both been reported following the integration of plasmonic nanostructures within the organic active layer. Most of these plasmonic OPV devices were fabricated either by blending randomly ordered metallic nanostructures within the active layer[5] or embedding them in a hole-transporting layer (PEDOT:PSS)[6]. A myriad of factors could be responsible for the inconsistent results – these include: metal absorption losses as well as backscattering losses by the metallic nanostructures near

the surface plasmon resonances (SPRs)[11,12]; morphology changes in the active material; improved/degenerated charge injection at the electrodes; modification of the carrier mobility[13,14]; and energy quenching[15] at the bare metal surface. Furthermore, the random distribution of plasmonic nanostructures would lead to inhomogenous broadening effects and depending on the species of the metal used, interaction and coupling between the nanostructures and metal electrodes (i.e., the Al cathode) could negate any enhancement, leading to low or reduced PCE[16,17]. Intricate details needed for device optimization may therefore be lost with the use of non-periodic plasmonic nanostructures.

Apart from the above issues, one pertinent challenge encountered by many researchers is the integration of a simple, cost-effective nano-lithography method for the preparation of periodic high-density nanostructures over large areas (e.g. typically ~9 mm^2 on an ITO substrate) with existing OSC fabrication processes. Masked techniques like extreme UV lithography would be too prohibitively expensive and direct-write techniques like electron beam lithography would be too time consuming – e.g., a nanodisk array with nanodisk diameter of 100 nm, and periodicity 300nm over a 9 mm^2 area would translate to ~10^{18} nanodisks. Demonstrating the feasibility of integrating a simple cost-effective, tailorable and scalable technique like nanosphere lithography (NSL) with existing OSC fabrication processes and investigating the origins of the efficiency enhancement in plasmonic OPV devices with a range of optical and electrical characterization techniques are the main foci of this work.

NSL, developed by Richard P. Van Duyne *et. al.*, provides an inexpensive, inherently parallel, high-throughput and broad material-compatibility approach for the fabrication large-scale, size-, and shape-tunable 2D periodic metallic nanostructure array.[18-20] Briefly, this technique is based on the self-assembly of a monodisperse layer of polystyrene or SiO_2 nanospheres, forming a well-packed hexagonal shadow mask for subsequent metal deposition. Following physical vapor deposition of metal over the spheres and the removal of the nanosphere mask, metal triangular nanostructures (nano-triangles (NTs)) are formed through the voids between the nanosphere lattice.

These metal nanostructures are expected to generate strong local fields due to their sharp edges. Previously, calculations based on the discrete dipole approximation method show an enhancement of surface-enhanced Raman spectroscopy on the order of 10^8 for NSL-derived triangle particles, which is much higher compared with other shapes, such as spheres ($\sim 10^2$) and tetrahedron ($\sim 10^4$).[21] Using photo-induced absorption spectroscopy, Kulkarni *et. al.* had earlier reported an enhanced generation of long-lived charge carriers in P3HT-PCBM films blended with Ag nanoprisms.[22]

Chang *et al.* [23] had earlier reported utilizing NSL to fabricate Ag nanoparticle array on the glass side of the organic thin-film solar cells to leverage on the surface plasmon resonant scattering. While this approach circumvents the integration issues of electrical shorts and energy quenching at the bare metal surface, one may not have utilized the full potential of the plasmonic nanostructures for light harvesting given the large separation between nanostructure array and the active organic layer (typically hundreds of microns for a typical glass substrate). Having the metal nanostructures in close proximity to the active area of the OPV devices pose great challenges for the device integration. Hence, till date, there have been no reports on the integration of NSL fabricated nanostructures on the ITO side of organic thin-film solar cells and photovoltaic performance evaluations of such devices. Herein, we fabricated large area, hexagonal arrays of Ag NTs on ITO substrates and integrated them in functional plasmonic OPV devices with Poly[[9-(1-octylnonyl)-9H-carbazole-2,7-diyl]-2,5-thiophenediyl-2,1,3-benzothiadiazole-4,7-diyl-2,5-thiophenediyl] : 1-(3-Methoxycarbonyl)-propyl-1-phenyl- (6,6)C61 (PCDTBT:PCBM) as the photoactive layer. The optical and photophysical properties of PCDTBT molecules near the Ag-NTs were investigated with both steady-state and transient optical spectroscopy and correlated with device performance data.

2. Experimental

2.1 Nano-triangle Fabrication

Mono-dispersed polystyrene spheres (200nm) in suspension (10% in water), purchased from PolySciences Inc., was diluted with an equal volume of ethanol[24]. A silicon substrate (3 cm × 3 cm) was cleaned by sonication sequentially in acetone, IPA, and deionized (DI)-water each for 5 mins followed by the immersion of the substrate in a 10% sodium dodecyl sulfate (SDS) solution for 24hrs. About 6 μL of the PS suspension was first applied onto the surface of the silicon substrate, which was then slowly slid into a tilted tray containing DI-water. A monolayer of PS spheres was formed on the surface of the water and the silicon substrate was then carefully removed. A few drops of 2% SDS solution were added to the water to promote the monolayer formation. The monolayer of self-assembled PS spheres on the water surface was then lifted up with a clean piece of ITO coated glass and dried in air. Next, a 20 nm thick Ag layer was deposited on the sample by vacuum evaporation. Following which, the PS sphere template was removed by immersing the sample in THF for 30 mins, followed by sonication for 1 min; leaving behind hexagonal arrays of Ag-NTs on the ITO substrate. For atomic force microscopy (AFM) and optical measurements, the Ag-NTs were prepared in the same manner, but transferred onto Si substrates and glass substrates respectively.

2.2 Atomic Force Microscopy and Optical Spectroscopy

The surface topography of the Ag-NTs array was imaged using an Asylum Research MFP-3D AFM in tapping mode. Steady-state absorption spectra were collected using a Shimadzu UV-3600 UV-VIS-NIR Spectrophotometer. Steady-state photoluminescence (PL) measurements were performed using a Horiba Jobin Yvon FL-1057 spectrofluorometer; while time-resolved photoluminescence (TRPL) measurements were performed using excitation pulses (400 nm or 500 nm, 150 fs) generated from a Coherent TOPAS-C^{TM} optical parametric amplifier that was pumped by a 1kHz Coherent Legend^{TM} regenerative amplifier and in turn seeded by a 80 MHz Coherent Vitesse^{TM} oscillator. Typically, the samples were photoexcited with a pump fluence of 1.5μJ/cm^2 and the TRPL signals were collected in a conventional backscattering geometry. The luminescence signal

was dispersed by a DK240 1/4 m monochromator with 300 g/mm grating and the temporal evolution of the PL was resolved by an Optronis Optoscope^{TM} streak camera system, which has an ultimate temporal resolution of ~10 ps when operated at the shortest time window of 330 ps. Nanosecond transient absorption spectroscopy (ns-TAS) were performed using an Applied Photophysics LKS.60 Nanosecond Laser Flash Photolysis Spectrometer with 500nm excitation pulses generated from a seed Nd:YAG, Q-switched laser (532 nm, 7 ns pulse width) and the probe is a 150 W Xe lamp aligned normal to the excitation source. Each time-resolved trace was acquired by averaging 50 laser shots at a repetition rate of 1 Hz. The typical laser pump fluence used is ~35 $\mu J/cm^2$. The data was collected in transmission geometry with the sample positioned at 45^o with respect to both the excitation source and probe light. All the spectroscopy was performed on freshly prepared samples.

2.3 OPV Device Fabrication and Characterization

The Ag-NTs integrated OPV cell was fabricated with the following device structure: glass / ITO / Ag-NTs / poly(3,4-ethylenedioxythiophene)-poly(styrenesulfonate) (PEDOT:PSS) / photoactive layer / Al – see Fig. 1(a). Reference cells without Ag-NTs were also fabricated for a comparative study. The PEDOT:PSS was first spincoated over the Ag-NTs on the ITO substrate as a planarization layer as well as to provide a buffer layer to prevent direct contact of the Ag-NTs with the photo-active layer, thereby mitigating any quenching effects at the bare metal surface. For all the samples, the Ag-NTs were covered with a 30nm thick PEDOT:PSS layer. The PEDOT:PSS coated substrate was subsequently annealed at 140°C for 10mins. The samples were then transferred into a nitrogen glove box to spincast the photoactive BHJ layers. The BHJ solution of PCDTBT (1-Materials): $PC_{61}BM$ (Nano-C) (1:4) prepared in chloroform with a concentration of 4mg/ml was then spincasted over the PEDOT:PSS layer. The thickness of photoactive films is ~60nm as measured by a surface profiler (Alpha Step IQ). The devices were completed with the deposition of a 100 nm thick Al cathode by thermal evaporation. The effective cell area defined by the geometrical overlap

between ITO and Al is ~0.071 cm^2. For steady-state absorption and nanosecond transient absorption, the samples (with and without Ag-NTs) were prepared on glass substrates without the Al cathode. For PL and TRPL characterization, PCDTBT only layers were prepared as the presence of any acceptor material (PCBM) will quench the fluorescence.

The current-voltage (I-V) characteristics of the devices in dark and under illumination were recorded with a HP 4155 semiconductor analyzer. The cells were illuminated by an Air Mass 1.5 Global (AM 1.5 G) solar simulator (San-ei XES-300, AAA rating) with an irradiation intensity of 1000W/m^2. The light intensity of the solar simulator was calibrated using a solarimeter with a reference silicon solar cell certified by National Renewable Energy Lab (NREL). The IPCE spectra were recorded using a Merlin radiometry system, where the light source is provided by a 150 W Newport-Oriel Xenon lamp, spectrally resolved using a Cornerstone 260 ¼ m monochromator and chopped at 60 Hz by an optical chopper. The light power-density was calibrated with a Hamamatsu silicon photodiode. All the device tests were performed in an inert nitrogen atmosphere.

3. Results and Discussions

3.1 AFM and Steady State Spectroscopy

Fig. 1(b) shows a typical AFM image of Ag-NT arrays where the height of the Ag triangles is measured to be ~20 nm. Each side of the triangle is ~40 nm as estimated from scanning electron microscopy micrographs (not shown). Fig. 2(a) shows the extinction spectra of PCDTBT:PCBM / PEDOT:PSS BHJ films with/without the Ag-NT array where the enhancement in the extinction over the spectral range (400 – 600 nm) matches that of the extinction spectrum of the Ag-NT array upon being embedded in a PEDOT:PSS layer as shown in Fig. 2(a) inset. The percentage enhancement in extinction is given in Fig. 2(b). The broad extinction peak can be attributed to the roughness of the glass substrate and the size distribution of the PS spheres (with a coefficient of variance of diameter ~8%). Steady state PL spectra of PCDTBT films in Fig. 3(a) show a broad featureless peak over the

spectral range of 620 – 760 nm following photoexcitation at 400 nm and 500 nm (Fig. 3(a) inset). Nonetheless, both spectra consistently exhibit a prominent PL enhancement in the samples with the Ag-NT array. Integrated PL intensity enhancements of 27% and 75% (over 620nm to 760nm) are estimated for the 400nm and 500nm excitations, respectively; in agreement with the larger extinction enhancement for the latter wavelength (i.e., 53%) as shown in Fig. 2(b). These results are consistent with two possibilities: (a) an increase of the local excitation field or (b) modifications to the exciton recombination rate. Transient optical spectroscopy would provide us with the answer to the origin(s) of the increase in extinction and PL enhancement.

3.2 Transient Optical Spectroscopy

Fig. 3(b) shows the TRPL decay transient for the freshly prepared PCDTBT/PEDOT:PSS films with and without the Ag-NT arrays following 400 nm excitation. The PL decay shown in Fig. 3(b) can be fitted by using multi-exponential function[6]:

$$I_{PL} = \sum_{i=1}^{n} A_i \exp(-\frac{t}{\tau_i})$$

where A_i is the amplitude of the i^{th} decay, τ_i is the i^{th} exponential constant. Over this timescale, the bare PCDTBT sample exhibits two lifetimes: τ_1 = 130 ± 50 ps and τ_2 = 620 ± 50 ps, with the former being ascribed to the decay of excitons that are not fully relaxed and the latter to the fully relaxed ones.[25] The measured lifetimes are comparable to those reported in the literature.[25] With the Ag-NTs embedded in the films, the fitted lifetimes are: τ_1 = 110 ± 50 ps and τ_2 = 590 ± 50 ps; which are comparable to the lifetimes in the bare PCDTBT sample (within the experimental uncertainty of the streak camera setup over the time window where the measurement was performed). With 10 nm of the PEDOT:PSS buffer layer separating the PCDTBT molecules and the Ag-NTs, exciton quenching is therefore not expected to have a dominant effect here. These TRPL results indicate that the exciton

lifetimes are not significantly affected by the presence of the Ag-NTs, thus pointing to scenario (a) above. This finding is in agreement with earlier reports on Ag/P3HT-PCBM systems in which there is negligible quenching of the P3HT excited states by the presence of Ag nanoprisms or Ag nanoparticles – i.e. consistent with a purely electromagnetic enhancement mechanism.[13,22,26] Hence, we relate the PL enhancement to originate from the LSPR of Ag-NT array. The LSPR of the Ag-NT array causes an increased absorption of PCDTBT by scattering and by strong near-field coupling near the resonance peak; resulting in a higher exciton generation rate and therefore higher PL intensities when they recombine.

To further validate these findings, we employed ns-TAS to probe the carrier dynamics of the PCDTBT:$PC_{61}BM$ blends in the ns to μs timescale over the spectral range of 530 – 650 nm . This technique is particularly suited for the study of charge recombination in BHJ cells. Fig. 4(a) and (b) shows the transient absorption spectra for the PCDTBT:PCBM / PEDOT:PSS BHJ films with/without the Ag-NT array and the relaxation dynamics of the negative ΔOD peak at ~580 nm (plotted as a decay transient). This negative ΔOD signal (i.e., a decreased absorption and increased transmission of light) over the spectral range of 530 – 650 nm originates from the ground state bleach (GSB) of the PCDTBT:PCBM blend following photoexcitation with 500 nm pulses.[27,28] Over this ns to μs timescale, this signal is attributed to the charge carriers (i.e., hole polarons) because in the blend, the singlet excitons are rapidly quenched by electron transfer from the PCDTBT to the PCBM and therefore the triplet exciton population is expected to be negligible.[28] Hence, the recovery (or the decay) of the ΔOD signal to the equilibrium can be attributed to the recombination of the hole polaron population and the magnitude of the ΔOD signal is therefore an indication of the population of photogenerated carriers in the sample.

Given that the thicknesses of the Ag-PCDTBT:PCBM and PCDTBT:PCBM films (i.e., the active layers, the buffer layer etc.) were carefully controlled to be the same, the larger magnitude of the ΔOD signal in the former (as seen in Fig. 4(a)) clearly indicates the presence of a larger hole

polaron population. This is consistent over the broad ns to μs timescale – see Fig. 4(b). The near invariance of the decay transients (monitored at 580 nm) in Fig. 4(c) clearly indicate that the hole polaron recombination dynamics are not significantly altered by the presence of the Ag-NT arrays. These ns-TAS results validate our earlier deduction that the presence of the Ag-NT array brings about an increased absorption in the PCDTBT:PCBM active layer by scattering and/or by strong near-field coupling near the resonance peak; resulting in a higher exciton generation rate and subsequently a higher population of hole polarons. Next, we shall correlate these findings from transient optical spectroscopy with the actual device performance of these samples to gain a deeper insight to the photophysical processes in plasmonics OSC devices.

3.3 Device Performance and IPCE Characterization

Fig. 6 shows the typical current-voltage (J-V) characteristics of OPV devices with and without Ag-NTs. The device parameters of these samples are tabulated in Table 1. The device performance of the reference cell (without Ag-NTs) is consistent with those values found in the literature[28-30]. With the integration of the Ag-NTs in the devices, the hybrid device exhibits an increase in PCE from 4.24% to 4.52%. This can be attributed to an enhancement of the short circuit current (J_{sc}) from -8.55 to -9.57 mA/cm^2. The open circuit voltage V_{OC} and the fill factor FF are comparable in the two samples, thereby validating the effectiveness of the PEDOT:PSS buffer layer in mitigating the charge recombination at the NTs. This observation also suggests that the charge injection at the PEDOT:PSS/ITO interface does not seem to be significantly affected by the presence of the NTs. The parameter J_{SC}, is dependent on generation and dissociation of excitons at the donor-acceptor interfaces and the subsequent charge collection at the electrodes. This enhancement in J_{sc} is consistent with the findings of increased hole polaron formation in the PCDTBT as revealed by ns-TAS measurements.

To evaluate the spectral dependence of the Ag-NTs on the photocurrent enhancement, the incident photon-to-electron conversion efficiency (IPCE) of the devices with and without Ag-NTs was measured (Fig. 6(b) inset) and the percentage enhancement was calculated by ($IPCE_{Ag\text{-}NTs}$ − $IPCE_{reference}$)/$IPCE_{reference}$ × 100%). A maximum enhancement (~20%) appears at around 510nm, which corresponds well with the LSPR of Ag-NTs embedded in PEDOT:PSS (Fig. 2(a) inset). Hence, it can be validated that the increase in the J_{SC} originates from the LSPR induced absorption enhancement of the PCDTBT: PCBM active layer. Our findings reveal a simple picture where the presence of Ag-NTs array increases the absorption in PCDTBT:PCBM by the strong local field and/or the scattering of the LSPR of Ag-NTs; thereby increasing the charge generation in the PCDTBT: PCBM based BHJ OPV devices.

4. Conclusions

In summary, we have demonstrated the feasibility of integrating a simple cost-effective, tailorable and scalable nano-lithography technique (nanosphere lithography) with existing OSC fabrication processes to realize plasmonic bulk heterojunction (PCDTBT:PCBM) organic solar cell. With the integration of the Ag-NTs on the ITO side in the devices, the plasmonic device exhibits an increase in PCE from 4.24% to 4.52%. and an increase in J_{sc} by ~12%. The comparable V_{OC} and FF of the conventional and plasmonic OPV device indicates that the PEDOT:PSS layer is effective in suppressing the charge recombination at the bare metal surfaces and the charge injection at the PEDOT:PSS/ITO interface is not adversely effected by the presence of the NTs. From a range of optical spectroscopy techniques (i.e., steady-state PL, TRPL and ns-TAS) and electrical characterization techniques (i.e., J-V and IPCE), we therefore attribute the improvements in the PCE to arise from an increase in exciton generation induced by the strong local E-field and/or scattering generated by the localized surface Plasmon resonance of the triangle arrays.

Acknowledgements

The work is supported by the Singapore National Research Foundation through the Competitive Research Programme under Project No. NRF-CRP5-2009-04 (X. Liu and T. C. Sum). T. C. Sum acknowledges the financial support from the Nanyang Technological University start-up grant (M58110068) and from the Ministry of Education (MOE) Academic Research Fund (AcRF) Tier 1 grant – RG 49/08 (M52110082).

References

(1) Park, S. H.; Roy, A.; Beaupre, S.; Cho, S.; Coates, N.; Moon, J. S.; Moses, D.; Leclerc, M.; Lee, K.; Heeger, A. J. *Nat. Photonics* **2009**, *3*, 297.

(2) Liang, Y.; Xu, Z.; Xia, J.; Tsai, S.-T.; Wu, Y.; Li, G.; Ray, C.; Yu, L. *Adv. Mater.* **2010**, *22*, E135.

(3) Shrotriya, V.; Wu, E. H. E.; Li, G.; Yao, Y.; Yang, Y. *Appl. Phys. Lett.* **2006**, *88*, 064104

(4) Atwater, H. A.; Polman, A. *Nat. Mater.* **2010**, *9*, 205.

(5) Kim, C.-H.; Cha, S.-H.; Kim, S. C.; Song, M.; Lee, J.; Shin, W. S.; Moon, S.-J.; Bahng, J. H.; Kotov, N. A.; Jin, S.-H. *ACS Nano* **2011**, *5*, 3319.

(6) Wu, J.-L.; Chen, F.-C.; Hsiao, Y.-S.; Chien, F.-C.; Chen, P.; Kuo, C.-H.; Huang, M. H.; Hsu, C.-S. *ACS Nano* **2011**, *5*, 959.

(7) Oo, T. Z.; Mathews, N.; Xing, G.; Wu, B.; Xing, B.; Wong, L. H.; Sum, T. C.; Mhaisalkar, S. G. *J. Phys. Chem. C* **2012**, *116*, 6453.

(8) Mapel, J. K.; Singh, M.; Baldo, M. A.; Celebi, K. *Appl. Phys. Lett.* **2007**, *90*, 121102.

(9) Tvingstedt, K.; Persson, N.-K.; Inganas, O.; Rahachou, A.; Zozoulenko, I. V. *Appl. Phys. Lett.* **2007**, *91*, 113514.

(10) Heidel, T. D.; Mapel, J. K.; Singh, M.; Celebi, K.; Baldo, M. A. *Appl. Phys. Lett.* **2007**, *91*, 093506.

(11) Beck, F. J. *J. Appl. Phys.* **2009**, *105*, 114310.

(12) Ferry, V. E.; Verschuuren, M. A.; Li, H. B. T.; Verhagen, E.; Walters, R. J.; Schropp, R. E. I.; Atwater, H. A.; Polman, A. *Opt. Express* **2010**, *18*, A237.

(13) Xue, M. *Appl. Phys. Lett.* **2011**, *98*, 253302.

(14) Kim, K. *Appl. Phys. Lett.* **2005**, *87*, 203113.

(15) Topp, K.; Borchert, H.; Johnen, F.; Tunc, A. V.; Knipper, M.; von Hauff, E.; Parisi, J.; Al-Shamery, K. *J. Phys. Chem. A* **2009**, *114*, 3981.

(16) Diukman, I.; Tzabari, L.; Berkovitch, N.; Tessler, N.; Orenstein, M. *Opt. Express* **2011**, *19*, A64.

(17) Tsai, S.-J.; Ballarotto, M.; Romero, D. B.; Herman, W. N.; Kan, H.-C.; Phaneuf, R. J. *Opt. Express* **2010**, *18*, A528.

(18) Haynes, C. L.; Van Duyne, R. P. *J. Phys. Chem. B* **2001**, *105*, 5599.

(19) Hulteen, J. C.; Van Duyne, R. P. *J. Vac. Sci. Technol., A* **1995**, *13*, 1553.

(20) Hulteen, J. C.; Treichel, D. A.; Smith, M. T.; Duval, M. L.; Jensen, T. R.; Van Duyne, R. P. *J. Phys. Chem. B* **1999**, *103*, 3854.

(21) Amanda J. Haes, C. L. H., Adam D. McFarland, George C. Schatz, Richard P. Van Duyne, Shengli Zou *MRS Bull.* **2005**, *30*, 368.

(22) Kulkarni, A. P.; Noone, K. M.; Munechika, K.; Guyer, S. R.; Ginger, D. S. *Nano Lett.* **2010**, *10*, 1501.

(23) Chang, Y. C.; Chou, F. Y.; Yeh, P. H.; Chen, H. W.; Chang, S. H.; Lan, Y. C.; Guo, T. F.; Tsai, T. C.; Lee, C. T. *J. Vac. Sci. Technol., B* **2007**, *25*, 1899.

(24) Cong, C.; Junus, W.; Shen, Z.; Yu, T. *Nanoscale Res. Lett.* **2009**, *4*, 1324

(25) Banerji, N.; Cowan, S.; Leclerc, M.; Vauthey, E.; Heeger, A. J. *J. Am. Chem. Soc.* **2010**, *132*, 17459.

(26) Stavytska-Barba, M.; Salvador, M.; Kulkarni, A.; Ginger, D. S.; Kelley, A. M. *J. Phys. Chem. C* **2011**, *115*, 20788.

(27) Marsh, R. A.; Hodgkiss, J. M.; Albert-Seifried, S.; Friend, R. H. *Nano Lett.* **2010**, *10*, 923.

(28) Etzold, F.; Howard, I. A.; Mauer, R.; Meister, M.; Kim, T.-D.; Lee, K.-S.; Baek, N. S.; Laquai, F. d. r. *J. Am. Chem. Soc.* **2011**, *133*, 9469.

(29) Blouin, N.; Michaud, A.; Leclerc, M. *Adv. Mater.* **2007**, *19*, 2295.

(30) Chu, T.-Y.; Alem, S.; Verly, P. G.; Wakim, S.; Lu, J.; Tao, Y.; Beaupre, S.; Leclerc, M.; Belanger, F.; Desilets, D.; Rodman, S.; Waller, D.; Gaudiana, R. *Appl. Phys. Lett.* **2009**, *95*, 063304.

Table 1: A comparison of the PCE, J_{sc}, V_{OC}, FF of the OPV devices with/without Ag-NTs

	PCE (%)	J_{sc} (mA/cm^2)	V_{oc} (V)	FF
With Ag-NTs	4.52	-9.57	0.89	0.53
Reference	4.24	-8.55	0.90	0.55

Fig. 1

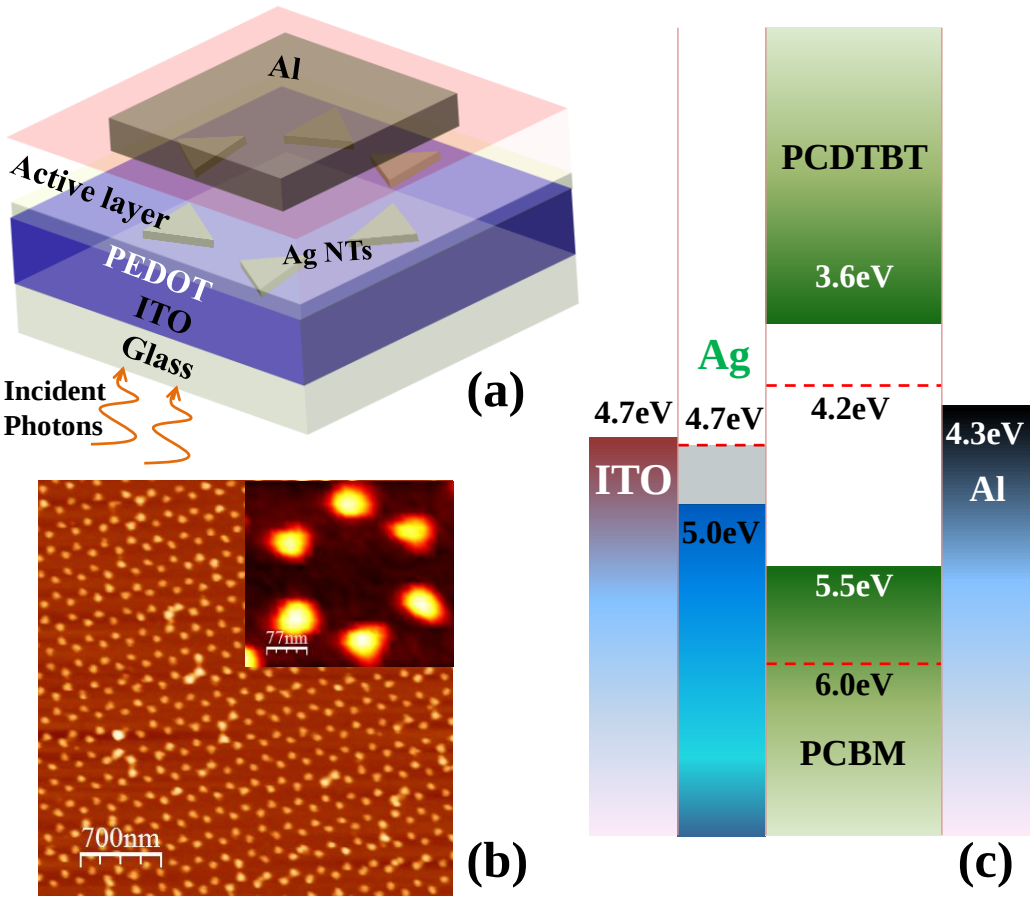

Fig1. (a) A schematic of the plasmonic organic photovoltaic device configuration investigated in our study. (b) AFM images of Ag-NT arrays. The height and side of the Ag triangles is ~20 nm and ~40 nm, respectively. Inset is a zoom-in of a representative unit of Ag-NT hexagonal array. (c) A schematic of the energy band alignment of the device.

Fig. 2

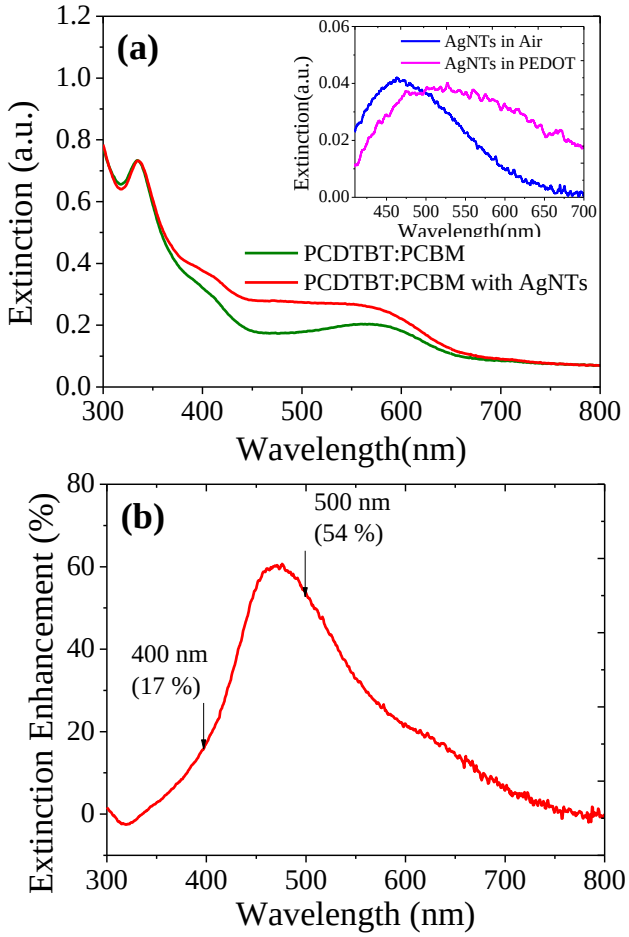

Fig2. (a) Extinction spectra of the PCDTBT:PCBM bulk-heterojunction films with/without Ag-NTs on glass substrate. Inset shows the extinction spectra of Ag-NTs on glass before and after spincoating PEDOT:PSS. The extinction spectrum of the Ag-NT array in air exhibits a broad surface plasmon resonance peak at ~465 nm which redshifts to ~500 nm upon being embedded in a PEDOT:PSS layer. (b) The relative enhancement in extinction for the PCDTBT:PCBM bulk-heterojunction films with Ag-NTs over the reference (without Ag-NTs) on glass substrate.

Fig. 3

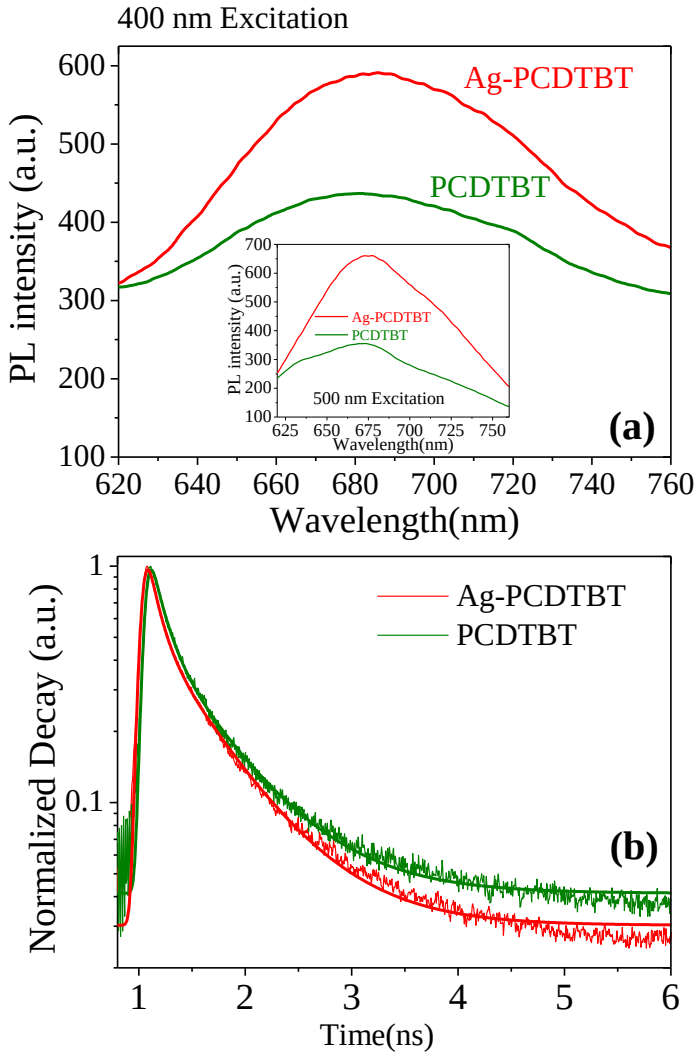

Fig3. (a) Steady-state PL of PCDTBT on glass substrate with/without Ag-NTs excited at (a) 400nm. Inset shows the PL of PCDTBT with/withoug Ag-NTs excited at 500nm. (b) Time-resolved photoluminescence of PCDTBT on glass substrate with/without Ag-NTs excited at 400nm at a fluence of 1.5 $\mu J/cm^2$. Similar decay transients were obtained for 500 nm excitation. Note that a layer of PEDOT:PSS was spincasted over the substrate or the Ag-NTs in all these samples.

Fig. 4

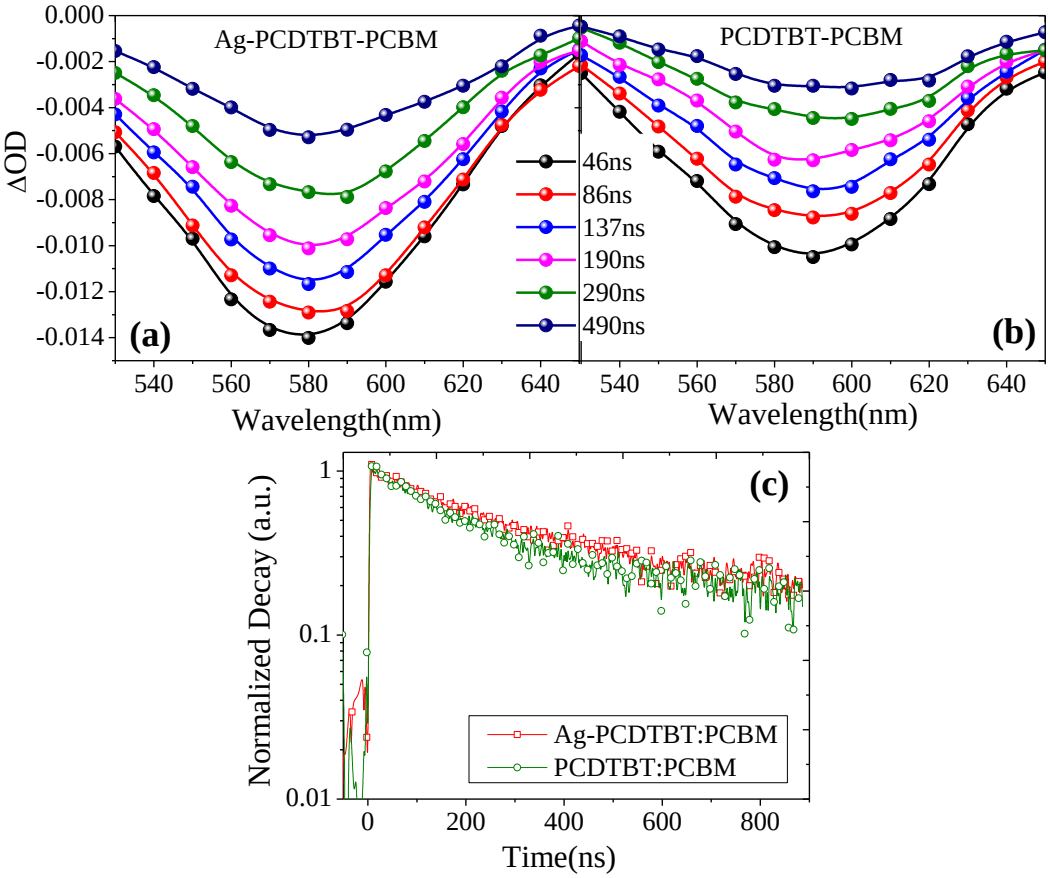

Fig4. ns-TAS spectra of PCDTBT:PCBM bulk-heterojunction films (a) with and (b) without Ag-NTs on a glass substrate. (c) The normalized decay of the two samples at 580nm, showing near invariance of the transient decay dynamics for the samples with and without Ag-NTs.

Fig. 5

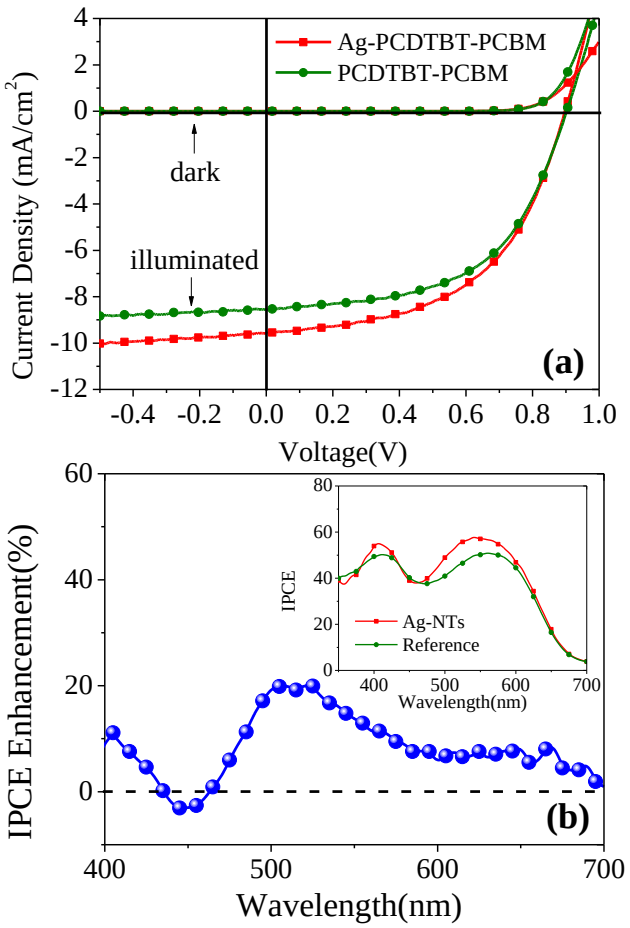

Fig5. (a) J-V characteristics of PCDTBT:PCBM BHJ OPV device with/ without Ag-NTs (b) The percentage enhancement in the IPCE of the devices with Ag-NTs over the reference (without Ag-NTs). Inset shows the IPCE of the two devices.

TOC